**EPJ manuscript No.**
(will be inserted by the editor)

# Knockout of proton-neutron pairs from $^{16}$O with electromagnetic probes

D.G. Middleton[1], J.R.M. Annand[2], C. Barbieri[3], C. Giusti[4], P. Grabmayr[1], T. Hehl[1], I.J.D. MacGregor[2], I. Martin[1], J.C. McGeorge[2], F. Moschini[1], F.D. Pacati[4], M. Schwamb[5], and D. Watts[6]

1 Kepler Centre for Astro and Particle Physics, Physikalisches Institut, Universität Tübingen, D-72076 Tübingen, Germany
2 Department of Physics and Astronomy, University of Glasgow, Glasgow G12 8QQ, Scotland
3 Theoretical Nuclear Physics Laboratory, RIKEN Nishina Center, Wako 351-0198, Japan
4 Dipartimento di Fisica Nucleare e Teorica dell'Università degli Studi di Pavia and Istituto Nazionale di Fisica Nucleare, Sezione di Pavia, I-27100 Pavia, Italy
5 Institut für Kernphysik, Johannes-Gutenberg Universität Mainz, Johann-Joachim-Becher-Weg 45, D-55099 Mainz, Germany
6 School of Physics, University of Edinburgh, Edinburgh, United Kingdom

Received: date / Revised version: date

**Abstract.** After recent improvements to the Pavia model of two-nucleon knockout from $^{16}$O with electromagnetic probes the calculated cross sections are compared to experimental data from such reactions. Comparison with data from a measurement of the $^{16}$O(e,e′pn) reaction cross section show much better agreement between experiment and theory than was previously observed. In a comparison with recent data from a measurement of the $^{16}$O($\gamma$,pn) reaction cross section the model over-predicts the measured cross section at low missing momentum.

**PACS.** 21.30.Fe Forces in hadronic systems and effective interactions – 21.60.-n Nuclear structure models and methods – 25.20.Lj Photoproduction reactions – 25.30.Fj Inelastic electron scattering to continuum

## 1 Introduction

A major quest of nuclear physics is to understand how the properties of nuclei arise from the underlying nucleon-nucleon (NN) interaction. A useful starting point is given by the independent particle models (IPM), in which protons and neutrons move freely in a common mean field. If one accounts for spin-orbit effects and the average effects of the tensor interaction [1], this approach explains the shell ordering of most stable and dripline isotopes. However, this picture cannot describe other basic observations, such as the strong fragmentation of nuclear spectra and the corresponding quenching observed for absolute spectroscopic factors [2]. The failure of the IPM arises from the correlated behaviour between nucleons, which, at short inter-nucleon separations, is characterised by a strong repulsion and, at intermediate to long range separations, by an attractive interaction dominated by complicated tensor and spin-orbit terms. Thus, to understand nuclear structure a careful study of this correlated behaviour is vital [3,4].

A direct method to study NN-correlations is by the use of two-nucleon knockout reactions with an electromagnetic probe [5]. Proton-proton and proton-neutron knockout reactions can act to probe the short range and tensor components of the NN-interaction, respectively. Real and virtual photons provide different and complementary information on the reaction process. Real photons are only sensitive to transverse components of the interaction while virtual photons are sensitive to both the transverse and longitudinal components.

Electromagnetically induced two-nucleon knockout reactions are driven by several processes. The coupling of the (real or virtual) photon to either nucleon of a correlated pair via one-body hadronic currents can lead to the ejection of both nucleons from the nucleus. Interaction of the photon with two-body hadronic currents such as meson exchange currents or isobar currents (IC) also contributes to the cross section. In addition final state interactions (FSI) between the two ejected nucleons and the recoil nucleus need to be taken into account. The relative importance of these different processes depends on the reaction type and kinematics.

Several past studies have focussed on the correlated behaviour of $^{16}$O since this nucleus is both convenient experimentally and can be approached with a variety of theoretical models [6–8]. There have been numerous measurements of two-nucleon knockout reactions at low energies using both real and virtual photons [9–15]. Refs. [11, 12, 10] focussed on two-proton emission and gave the first evidence of short-range correlations in nuclei. More recently, high-energy electron scattering at Jefferson Laboratory [16] focussed on the strength of short-range correlations in both the central and tensor channels. These studies put in evidence that, at short distances, proton-neutron pairs are more correlated than proton-proton ones due to tensor effects. In a recent calculation [17] both the $^{16}$O(e,e′pp)$^{14}$C and $^{16}$O(e,e′pn)$^{14}$N were studied by combining the self-consistent Green's function theory for correlations and the Pavia model for the reaction mechanism. These calculations suggest that the emission of a proton-neutron pair at lower energy is strongest in the $1^+$ channel, indicating again the importance of tensor correlations. However, it was later seen that the cross section are sensible to the long-range details of the correlated wave function, rather than short-range correlations [6]. Thus, new and important information could be extracted if one is able to disentangle the contribution of the various currents to the cross sections. To test reaction models, comparisons with data is important.

The results of [17] were compared with the first measurement of the $^{16}$O(e,e′pn)$^{14}$N reaction in [9]. However, the theorerical calculations did not reproduce the shape or the magnitude of the data. These discrepancies sparked further developments to improve the reaction model with respect to the treatment of FSI [18,19], of the two-body currents [20], and of the centre-of-mass (CM) effects in the hadronic (or ELECTROMAGNETIC????) current (HC) operator [6,21][1]. This paper presents a new comparison between experimental data and recent calculations [6], and shows that the hadronic (or ELECTROMAGNETIC????) current's CM (HCCM) effects resolve the discrepancy found in [9]. At the same time, calculated cross sections for the similar $^{16}$O($\gamma$,pn)$^{14}$N reactions are compared to new data from a recent measurement [22]. For these, however, discrepancies still persist.

## 2 Theoretical calculations

The cross section of a reaction induced by a real or virtual photon, with momentum $\boldsymbol{q}$, where two nucleons are ejected from a nucleus can be written in terms of the transition matrix elements of the nuclear current operator between initial and final nuclear states. Bilinear products of these matrix elements give the components of the hadron tensor and therefore the cross section [5]. For an exclusive process, where the residual nucleus is left in a discrete eigenstate of its Hamiltonian, and under the assumption of a direct knock-out mechanism, the transition matrix elements contain three main ingredients: the two-nucleon overlap function between the ground state of the target and the final state of the residual nucleus, the hadronic current, and the two-nucleon scattering wave function [23].

The two-nucleon overlap function (TOF) contains information on nuclear structure and correlations. In [6] different treatments of correlations are compared, and produce dramatic differences both in the shape and in the magnitude of the proton-neutron emission cross sections. In particular, a crucial role is played by tensor correlations. In the most refined approach, the TOF is obtained from a self-consistent calculation of the two-hole Green's function. In this case, the coupling of nucleons and collective excitations of the system is calculated microscopically from realistic NN forces. This is done employing the Faddeev random phase approximation (FRPA) method discussed in [24–27]. The long-range part of tensor correlations is also included explicitly. The TOF has been calculated in [17] by partitioning the Hilbert space. Long-range correlations are evaluated using FRPA and the Bonn-C NN-potential [28,29] in an appropriate harmonic oscillator basis. The effects of short-range correlations, due to the central and tensor part at high momenta, lie outside this space. Thus they were added by computing the appropriate defect functions.

The nuclear current is the sum of a one-body and a two-body contribution. The one-body current includes the longitudinal charge term and the transverse convective and spin currents. The two-body current is derived from a non relativistic reduction of the lowest-order Feynman diagrams with one-pion exchange and includes terms corresponding to the $\pi$-seagull and pion-in-flight diagrams, and to the diagrams with intermediate $\Delta$-isobar configurations. Details of the nuclear current components can be found in [20,30,31]. In comparison with the previous calculations of [9], the regulaization of the two-body current has been improved using a dipole cut-off consistent with the Bonn-C interaction (which is also employed in calculating the initial state correlations) [6].
[[Carlotta: can we say "consistent"??? Or is it safer to change to "the same dipole cut-off of the Bonn-C..."???]]

The two-nucleon scattering wave function contains the interaction of each one of the two outgoing nucleons with the residual nucleus, described in the model by an optical potential, as well as the mutual interaction of the two ejected nucleons (NN-FSI). We have first performed simplified calculations in which only the core-nucleon interactions are taken into account. The scattering state is then written as the product of two uncoupled single particle distorted wave (DW) functions, eigenfunctions of a complex phenomenological optical potential which contains a central, a Coulomb, and a spin-orbit term. In the more complete approach (which we will refer to as DW-NN) the contribution of NN-FSI is also included within the perturbative approach reported in [18,19].

In comparison with earlier studies, we include correctly the center of mass effect on the hadronic (or ELECTROMAGNETIC????) current (HCCM) [6,21]. Calculations are performed in the CM frame, where the transition operator becomes a two-body operator even in the case of a one-body hadronic current. Unfortunately, this process introduces a spurious contribution due the lack of orthogonality between the bound and scattering states (which are obtained from an energy-dependent optical potential). This issue arises *only* for the one-body currents and, in the previous calculations for proton-neutron knockout [9, 17], was addressed by neglecting altogether the HCCM correction of the one-body current. This approximation

[1] Note that this effects is different form the recoil of the residual nucleus, which contributes only at the order of a few percent.

was deemed to be small in most previous studies. However, Refs. [6,21] have shown that such effects actually depend on the kinematics and may become large in certain cases. The issue has eventually been overcome in [6] by enforcing orthogonality between single particle initial and final states by means of the Gram-Schmidt procedure. Therefore it is no longer a problem to include the HCCM effect correctly. The calculations of Ref. [21] show that this effect is indeed negligible [[CARLOTTA please check these statements!!!]] for $^{16}$O(e,e$'$pp)$^{14}$C reactions in the kinematics of Refs. [11,12], while it may slightly improve the comparison with he data of Refs. [10]. Therefore HCCM do not affect the conclusion of these references. The situation is diferent for the particular case of super-parallel kinematics, which were used in the measurement of the $^{16}$O(e,e$'$pn)$^{14}$N reaction [9]. Here, he HCCM effect enhance the contribution to the cross section which arises from the one-body currents. This effect is dramatic at low missing momentum. The comparison between the $^{16}$O(e,e$'$pn)$^{14}$N data and the correct calculations is reported in Sec. 4.1 and shows that HCCM resolve the previously observed [9] discrepancy with experiment.

## 3 Experimental set-up

### 3.1 The $^{16}$O(e,e$'$pn)$^{14}$N reaction

A first measurement of $^{16}$O(e,e$'$pn)$^{14}$N reaction [9] was made at the electron scattering facility (3-spectrometer facility [32]) at MAMI, Mainz [33,34]. Data were taken with an incoming electron beam of energy 855 MeV at currents of 10-20 $\mu$A. The beam was incident upon a waterfall target [35] of thickness 74 mg cm$^{-2}$. The data were collected at energy and momentum transfers of 215 MeV and 316 MeV/$c$ where the ejected proton was detected in the forward direction, parallel to $\boldsymbol{q}$, with the ejected neutron detected in the backward direction, anti-parallel to $\boldsymbol{q}$, in so called "super-parallel" kinematics. The ejected proton and scattered electron were detected with Spectrometers A and B [32] of the 3-spectrometer set-up while the ejected neutron was detected using the Glasgow-Tübingen time-of-flight detector system [36]. Further details about the experimental set-up and analysis of the data can be found in ref. [9]. The experimental resolution of the set-up was sufficient to distinguish groups of states in the residual nucleus but not good enough to separate individual states.

### 3.2 The $^{16}$O($\gamma$,pn)$^{14}$N reaction

The $^{16}$O($\gamma$,pn)$^{14}$N reaction cross section was measured at the Glasgow photon tagging facility [37,38] at MAMI, Mainz [33,34]. An electron beam of energy 855 MeV used at a current of 50 nA was incident upon a 4 $\mu$m Nickel radiator to produce tagged Bremsstrahlung photons in the energy range 100 to 800 MeV. The Glasgow-tagger has an energy resolution of 2 MeV. The tagged photons, collimated to a diameter of 18 mm, were incident upon a target of 1 mm thickness. The target cell was filled with deuterated water and consisted of an Aluminium frame with polythene foil windows of 30 $\mu$m thickness which was orientated at an angle of 30° with respect to the photon beam.

The ejected protons were detected in an array of four hyper-pure Germanium detectors (HPGe) of the Edinburgh Ge6-Array [39], each of which covered a solid angle of 59 msr and had a proton energy acceptance of 18 - 250 MeV. Pairs of double sided silicon strip detectors [22] positioned in front of the HPGe detectors were used to determine the trajectory of the ejected protons and reconstruct the reaction vertex. The ejected neutrons were detected at forward angles using the Glasgow-Tübingen time-of-flight detectors [36]. Five neutron detector stands were used which covered an in-plane polar angular range of $6 - 53°$ and a total solid angle of 146 msr. A pulse-height threshold of 5 MeV$_{ee}$ was used in the neutron detectors which resulted in a neutron kinetic energy threshold of ≈10 MeV. Full details of the experimental set-up and analysis of the data can be found in [22]. The experimental resolution of the set-up was not sufficient to resolve individual excited states in the residual $^{14}$N nucleus, only groups of states.

## 4 Results

### 4.1 The $^{16}$O(e,e$'$pn)$^{14}$N reaction

Figure 1 shows the experimental and theoretical cross sections for the $^{16}$O(e,e$'$pn)$^{14}$N reaction as a function of the absolute magnitude of the missing momentum $\boldsymbol{p}_{\mathrm{m}} = \boldsymbol{q} - \boldsymbol{p'}_{\mathrm{p}} - \boldsymbol{p'}_{\mathrm{n}}$, where $\boldsymbol{p'}_{\mathrm{p}}$ and $\boldsymbol{p'}_{\mathrm{n}}$ are the momenta of the ejected nucleons. The experimental cross section has been determined for a group of states in the residual $^{14}$N for an excitation energy range of 2 to 9 MeV. The theoretical curves are the result of DW calculations and are the average cross section of calculations for the kinematic settings as given in [9]. The calculations represent the sum of contributions for transitions to three excited states in $^{14}$N: the 2.31 MeV ($0^+$), 3.95 MeV ($1^+$) and 7.03 MeV ($2^+$) states.

The theoretical curves of fig. 1 also show the contributions of different terms of the nuclear current to the cross section. Cumulative contributions of the one-body, $\pi$-seagull, pion-in-flight and isobar currents are all shown. At low missing momentum the largest contribution to the theoretical cross section is from one-body hadronic currents. Above $p_{\mathrm{m}} = 150$ MeV/$c$ the $\pi$-seagull and ICs become increasingly more important with increasing $p_{\mathrm{m}}$. The pion-in-flight contribution is relatively small over the whole missing momentum range shown.

The shape of the experimental and theoretical cross sections in fig. 1 show reasonable agreement in that they both decrease roughly exponentially with increasing $p_{\mathrm{m}}$ and both show a flattening in the cross section at $p_{\mathrm{m}} \approx 175$ MeV/$c$. The magnitude of the two cross sections is in much better agreement compared to a previous comparison in [9] where the theoretical calculations under-

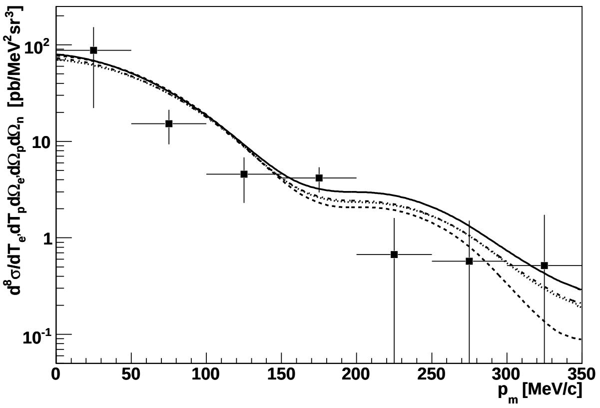


**Fig. 1.** The $^{16}$O(e,e′pn)$^{14}$N cross section shown as a function of the missing momentum for events in the range $2 \leq E_x \leq 9$ MeV for energy and momentum transfers of 215 MeV and 316 MeV/$c$. The curves show the results from theoretical calculations of the cross section which includes transitions to the first three excited states in $^{14}$N, 2.31 MeV ($0^+$), 3.95 MeV ($1^+$) and 7.03 ($2^+$). The dashed line is calculated only with the one-body currents; the dotted line also includes the $\pi$-seagull term; the dashed dotted includes the one-body, $\pi$-seagull term and pion-in-flight terms and the solid line is for the complete cross-section including contributions from IC.

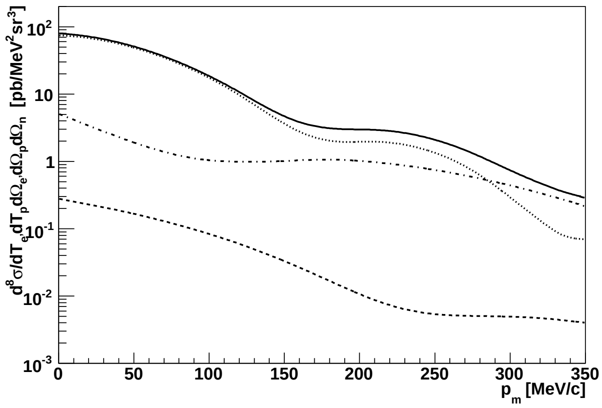


**Fig. 2.** Theoretical $^{16}$O(e,e′pn)$^{14}$N cross sections for energy and momentum transfers of 215 MeV and 316 MeV/$c$. The 2.31 MeV ($0^+$), 3.95 MeV ($1^+$), 7.03 ($2^+$) and the three states combined, represented by the dashed, dotted, dashed-dotted and solid lines respectively. The plots are for the full cross section including the one-body, $\pi$-seagull, pion-in-flight and IC terms.

predicted the experimental data at low $p_{\rm m}$. This improvement is due to the enhancement, at low $p_{\rm m}$, of the contribution from the one-body currents produced by the CM effects included in the present model [6].

Figure 2 shows a comparison of calculations of the full cross sections, including the one-body and two-body currents, for transitions to the three different excited states included in the curves of fig. 1. The main strength in the cross section is predicted to come from transitions to the 3.95 MeV ($1^+$) state up to $p_{\rm m} \approx 290\,{\rm MeV}/c$ where transitions to the 7.03 ($2^+$) state become dominant. The calculated contribution from transitions to the 2.31 MeV ($0^+$) state is at least an order of magnitude weaker, over the full $p_{\rm m}$ range shown, than those involving transitions to either of the other two states.

The calculations in figs. 1 and 2 are performed in the DW approach for FSI. NN-FSI effects depend on kinematics and on the reaction type and are generally small in proton-neutron emission [18,19]. For the $^{16}$O(e,e′pn)$^{14}$N reaction in the super-parallel kinematics NN-FSI are small but not negligible [6]. The effect of the mutual interaction between the two outgoing nucleons is shown in fig. 3, where the cross sections obtained in the DW and DW-NN approaches are compared for transitions to the 3.95 MeV ($1^+$) state in $^{14}$N. This one state dominates the reaction over nearly all of the measured $p_{\rm m}$ range. The effects of NN-FSI on the calculated cross section are relatively small. There is a slight decrease in cross section for $p_{\rm m} \leq 50\,{\rm MeV}/c$ and a slight increase for $150 \leq p_{\rm m} \leq 225\,{\rm MeV}/c$ and above $p_{\rm m} = 300\,{\rm MeV}/c$. In general the calculations predict that NN-FSI have little importance

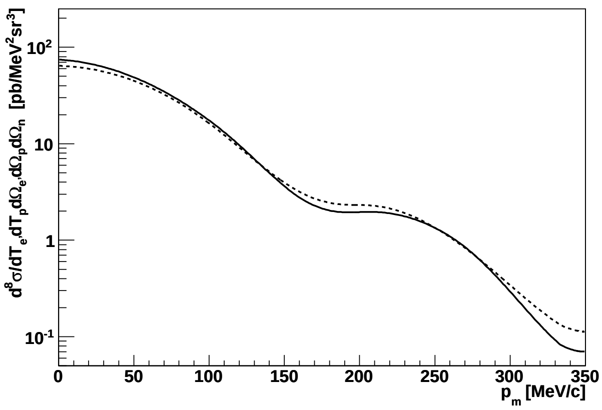


**Fig. 3.** Theoretical $^{16}$O(e,e′pn)$^{14}$N cross sections for transitions to the 3.95 MeV ($1^+$) excited state of $^{14}$N for energy and momentum transfers of 215 MeV and 316 MeV/$c$. The solid curve uses the DW approach, the dashed line the DW-NN approach for FSI.

for the kinematics shown here. This fact justifies the perturbative treatment of NN-FSI.

### 4.2 The $^{16}$O($\gamma$,pn)$^{14}$N reaction

Figure 4 shows the cross section for the $^{16}$O($\gamma$,pn)$^{14}$N as a function of the absolute magnitude of the missing momentum, $p_{\rm m}$, of the reaction. The data are shown for an incident photon energy range of $150 \leq E_\gamma \leq 250$ MeV, proton in-plane azimuthal acceptance of $142 \leq \theta_p \leq 158^\circ$ and neutron in-plane azimuthal acceptance of $8 \leq \theta_n \leq 32^\circ$. The experimental cross section has been determined for a group of states in the recoiling $^{14}$N nucleus for an excitation energy range of 2 to 10 MeV. Figure 4 also shows

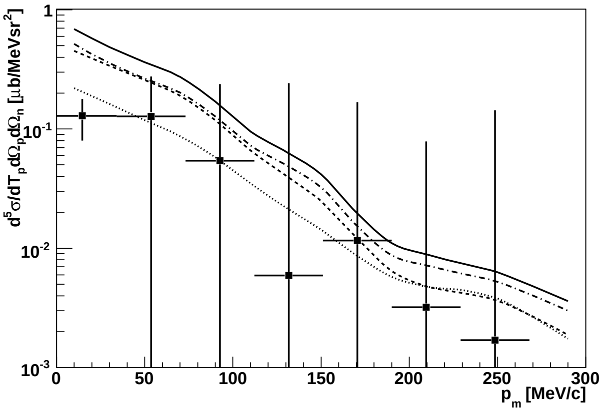


**Fig. 4.** The $^{16}$O($\gamma$,pn)$^{14}$N cross section as a function of the missing momentum for events in the range $2 \leq E_x \leq 10$ MeV. The incident photon energy range was $150 \leq E_\gamma \leq 250$ MeV. The curves show the theoretical cross section for transitions to the 3.95 MeV ($1^+$) state. The dashed line is calculated with only one-body currents included; the dotted line also includes the $\pi$-seagull term; the dashed dotted includes the one-body, $\pi$-seagull term and pion-in-flight terms and the solid line is for the complete cross-section including contributions from IC.

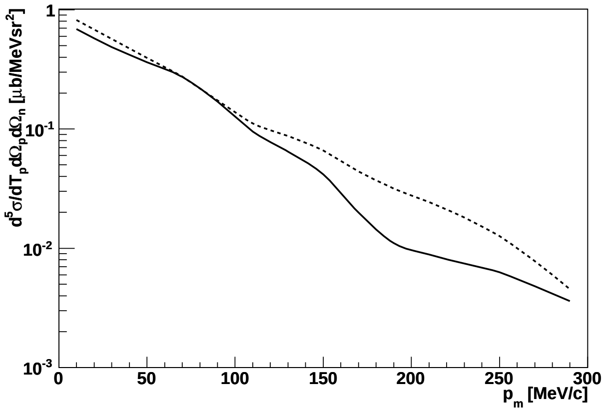


**Fig. 5.** Theoretical $^{16}$O($\gamma$pn)$^{14}$N cross sections for transitions to the 3.95 MeV ($1^+$) excited state of $^{14}$N. The solid curve uses the DW approach, the dashed line the DW-NN approach for FSI.

the results of DW theoretical calculations for the reaction. The curves are for transitions to the 3.95 MeV ($1^+$) state which is believed to dominate the cross section which the measurements in [14] suggest dominate the cross section and have been averaged over the kinematic settings which cover the acceptance of the experimental data.

The theoretical curves of fig. 4 show the contributions of different terms of the hadronic current to the cross section. Cumulative contributions of the one-body, $\pi$-seagull, pion-in-flight and isobar currents are all shown, see the caption of fig. 4 for details. At low $p_{\rm m}$ the largest contribution to the theoretical cross section is from one-body hadronic currents. The inclusion of the $\pi$-seagull term causes a decrease in calculated cross section until roughly $p_{\rm m} = 200$ MeV/$c$ where it has very little effect. The further inclusion of the pion-in-flight contributions increases the cross section to roughly the same strength as the one-body hadronic current cross section for $p_{\rm m} < 100$ MeV/$c$ after which point it increases the calculated cross section relative to the one-body hadronic currents alone. The inclusion of ICs increases the calculated cross section for the whole $p_{\rm m}$ range shown.

The effect of the mutual interaction between the two outgoing nucleons for the ($\gamma$,pn) reaction is shown in fig. 5. Theoretical cross sections were obtained using the DW and DW-NN approaches for transitions to the 3.95 MeV ($1^+$) state in $^{14}$N. At low $p_{\rm m}$ the effects of NN-FSI on the calculated cross section are very small. From about $p_{\rm m} = 100$ MeV/$c$ the importance of NN-FSI increases until roughly $p_{\rm m} = 200$ MeV/$c$ after which their importance again diminishes. This is in contrast to what was seen for the (e,e′pn) reaction where NN-FSI had very little effect on the calculated cross section. The inclusion of NN-FSI increases the theoretical cross section at high $p_{\rm m}$ which, however, remains well within the statistical error bars associated with the data points in this region. All calculations include properly the HCCM effect. Although, we have verified that this does not give substantial contributions for $^{16}$O($\gamma$,pn)$^{14}$N in the present kinematics.

For $p_{\rm m} > 50$ MeV/$c$, both the theoretical and experimental cross sections shown in Fig. 4 appear to have similar trends of falling roughly exponentially with increasing $p_{\rm m}$. With the the calculation being somewhat larger than the data. However, no definitive statement can be made due to the large error bars.

## 5 Conclusions

References [6,21] have overcome an approximation previously employed for calculating the hadronic [or electromagnetic?!?!?] current in the center-of-mass. This work performed a new comparison with the $^{16}$O(e,e′pn)$^{14}$N data and showed that this HCCM effect solves a previous discrepancy with between theory and experiment, with both the shape and magnitude of the experimental cross section being well described. Moreover, this correction does not affect the conclusions of previous two-proton emission experiments [11,12,10].

We have also presented new data on proton-neutron emission extracted from the $^{16}$O($\gamma$,pn)$^{14}$N reaction and extended our comparison to this. In this case, the theoretical calculations appear to over-predicts the data, althoguh only one point at low $p_{\rm m}$ is clearly calculated outside the experimental error bars.

The theoretical model employed in this work is already very sophisticated in the treatment of the reaction process and includes the most complete microscopical study initial correlations possible to date. Calculations made in several kinematics [6] suggests that in principle it would be possible to extract information on long-range tensor correlations from proton-neutron emission. However, this requires a larger amount of experimental data. With the present statistics, a good agreement with the (e,e′pn) and the reproduction of at least for the order of magnitude for ($\gamma$,pn) should be considered as a positive test of the model for the reaction mechanism.

Obviously, the $^{16}$O($\gamma$,pn)$^{14}$N reaction remains an open issue since theoretical calculations do not compare perfectly and appear to over-predicts the experiment at low $p_{\mathrm{m}}$. More accurate measurements are necessary to confirm this. However, if this discrepancy will persist, then it may indicate a the different response of the correlated pair to the longitudinal and transverse electromagnetic currents. This isinformation would be valuable to constrain the off-shell behavior of tensor correlations in the medium.

## Acknowledgments

The authors would like to thank the staff of the Institut für Kernphysik in Mainz for providing the facilities in which these experiments took place. This work was sponsored by the Deutsche Forschungsgemeinschaft and the UK Science and Technology Facilities Council (STFC). The work C.B. is supported by the Japanese Ministry of Education, Science and Technology (MEXT) under KAKENHI grant no. 21740213.

## References

1. T. Otsuka et al. *Phys. Rev. Lett.*, 95:232502, 2005.
2. L. Lapikás. *Nucl. Phys. A*, 553:297c, 1993.
3. H. Müther and A. Polls. *Prog. Part. Nucl. Phys.*, 45:243, 2000.
4. W.H. Dickhoff and C. Barbieri. *Prog. Part. Nucl. Phys.*, 52:377, 2004.
5. S. Boffi et. al. *Electromagnetic Response of Atomic Nuclei*. Oxford University Press, 1996.
6. C. Giusti et. al. *Eur. Phys. J. A*, 33:29, 2007.
7. J. Ryckebusch and W. Van Nespen. *Eur. Phys J. A*, 20:435, 2004.
8. M. Anguiano et. al. *Nucl. Phys. A*, 744:168, 2004.
9. D. G. Middleton et. al. *Eur. Phys. J. A*, 29:261, 2006.
10. G. Rosner. *Prog. Part. Nucl. Phys.*, 44:99, 2000.
11. C. J. G. Onderwater et. al. *Phys. Rev. Lett.*, 81:2213, 1998.
12. R. Starink et. al. *Phys. Lett. B*, 474:33, 2000.
13. I. J. D. MacGregor et. al. *Nucl. Phys. A*, 533:269, 1991.
14. L. Isaksson et. al. *Phys. Rev. Lett.*, 83:3146, 1999.
15. K. R. Garrow et. al. *Phys. Rev. C*, 64:064602, 2001.
16. R. Subedi et al. *Science*, 320:1476, 2008.
17. C. Barbieri et. al. *Phys. Rev. C*, 70:014606, 2004.
18. M. Schwamb et. al. *Eur. Phys. J. A*, 17:7, 2003.
19. M. Schwamb et. al. *Eur. Phys. J. A*, 20:233, 2004.
20. C. Giusti et. al. *Eur. Phys. J. A*, 26:209, 2005.
21. C. Giusti et. al. *Eur. Phys. J. A*, 31:155, 2007.
22. F. Moschini. *The high resolution $^{16}O(\gamma,pn)^{14}N$ reaction at MAMI*. PhD thesis, Universität Tübingen, 2007.
23. C. Giusti and F.D. Pacati. *Nucl. Phys. A*, 615:373, 1997.
24. C. Barbieri and W. H. Dickhoff. *Phys. Rev. C*, 63:034313, 2001.
25. C. Barbieri. *Phys. Lett. B*, 643:268, 2006.
26. C. Barbieri, D. Van Neck, and W. H. Dickhoff. *Phys. Rev. A*, 76:052503, 2007.
27. C. Barbieri and M. Hjorth-Jensen. *Phys. Rev. C*, 79:064313, 2009.
28. R. Machleidt et al. *Phys. Rep.*, 149:1, 1987.
29. R. Machleidt. *Adv. Nucl. Phys*, 19:189, 1989.
30. C. Giusti and F.D. Pacati. *Nucl. Phys. A*, 641:297, 1998.
31. P. Wilhelm et. al. *Z. Phys. A*, 359:467, 1997.
32. K. I. Blomqvist et al. *Nucl. Instr. and Meth. in Phys. Res. A*, 403:263, 1998.
33. Th. Walcher. *Prog. Part. Nucl. Phys.*, 24:189, 1990.
34. H. Herminghaus et. al. *Nucl. Instr. and Meth. in Phys. Res. A*, 138:1, 1976.
35. N. Voegler et al. *Nucl. Instr. and Meth.*, 198:293, 1982.
36. P. Grabmayr et al. *Nucl. Instr. and Meth. in Phys. Res. A*, 402:85, 1998.
37. I. Anthony et al. *Nucl. Instr. and Meth. in Phys. Res. A*, 301:230, 1991.
38. S.J. Hall et al. *Nucl. Instr. and Meth. in Phys. Res. A*, 368:698, 1996.
39. N. P. Harrington et al. *Phys. Rev. C*, 75:044311, 2007.